Electronic and impurity-induced Raman scattering in MgO:Co^{2+}

Soumyendu Guha
Instituto de Física, UNICAMP-Campinas, São Paulo, Brazil
(Received 17 September 1979)

Theoretical and experimental Raman-scattering studies of impurity-induced vibrations have been carried out in MgO:Co^{2+}. The experimental spectra are taken as a function of temperature from 18 °K to room temperature. The temperature dependence of a peak at 935.7 cm^{-1} indicates that its origin is of electronic nature. We assign it to the $\tau_6 \rightarrow \tau_8^2$ transition between the low-lying energy levels of the Co^{2+} ion in cubic fields. Theoretical calculations for the Raman spectra are presented, assuming the electron-phonon interactions to be a linear function of the displacements of the defect's first-, second-, third-, and fourth-nearest neighbors. This assumption leads to a very good agreement of the line-shape and peak positions between theory and experiment. As an alternative model, we also consider the perturbed-phonon model in which changes of the longitudinal force constants between the defect and its nearest neighbors as well as nearest and fourth-nearest neighbors have been assumed. This model leads to an unsatisfactory agreement between theory and experiment.

I. INTRODUCTION

In crystals of rock-salt structure such as pure MgO, every ion is at its own inversion site. None of the zero-wave-vector ($\vec{q}=0$) phonons are of even parity and therefore, first-order Raman scattering is not allowed. However, when an impurity is introduced at a substitutional lattice site, the translational symmetry as well as the inversion symmetry is destroyed except at the impurity site. Thus, the $\vec{q}=0$ selection rule no longer holds and first-order Raman scattering is allowed. Numerous studies of first-order Raman spectra for a variety of crystals have revealed valuable information about the host lattice. The first-order Raman spectra also provide information about the electronic energy states of the defect when it is embedded in the host lattice at a substitutional lattice site. We report here an experimental and theoretical study of the first-order vibrational spectrum in MgO:Co^{2+}. We have also observed a strong peak at 935.7 cm^{-1}. From the temperature-dependence study of this peak, we assign it to an electronic transition ($\tau_6 \rightarrow \tau_8^2$) between the low-lying electronic states of the Co^{2+} ion in cubic fields. In an earlier paper, Billat *et al.*[1] have reported the first-order spectrum in this crystal at 77 °K. They have also calculated the first-order spectrum using the breathing-shell model (BSM) of Schroder *et al.*[2] However, their calculations lack the following details for which they were unable to produce the sharp features in the observed spectrum: (i) they used a mesh of 264 points in a 1/48th section of the Brillouin zone, corresponding to about 8000 points in the entire zone, and (ii) they assumed the electron-phonon interaction to be a linear function of the displacements of the defect's nearest neighbors.

We have reexamined the problem of the first-order Raman scattering in MgO:Co^{2+} for the following reasons: (i) Adopting the BSM calculations of Sangster *et al.*[3], we have obtained host-lattice phonon frequencies and polarization vectors for 1686 $\vec{q}$ vectors in the Kellermann 1/48 section of the Brillouin zone. Through symmetry operations, this is equivalent to a uniform mesh of 64 000 $\vec{q}$ vectors. This large number for the frequency mesh has enabled us to produce a more detailed and accurate theoretical spectrum compared to that of Billat *et al.*[1] (ii) It has been shown recently[4,5] that a significant improvement between theory and experiment is achieved when second- as well as first-nearest-neighbor displacements in the electron-phonon interaction are included. In this work, we include in our calculations fourth-, third-, second-, and first-nearest neighbor displacements in the electron-phonon interactions. (iii) We also examine the force-constant perturbation model of Gethin *et al.*,[6] in which a force-constant change between the nearest and fourth-nearest neighbor is assumed, in addition to the longitudinal-force-constant change between the defect and its nearest neighbors. (iv) We have conducted a temperature-dependent study from 18 °K to room temperature to identify the phonon and electronic Raman excitations.

II. THEORY

A. Green's-function matrix

In the perfect crystal, the equation of motion for a normal mode is given by

$$(\underline{A} - \omega^2 \underline{I})\underline{v} = 0 , \tag{1}$$

where $\underline{A}$ represents the harmonic-coupling-constant matrix and $\underline{I}$ is the unitary matrix. The ei-

genvalues will be denoted by $\omega_{q\lambda}^2$ and the orthonormal phonon eigenvectors by $v_{q\lambda}$, with components given by

$$|q\lambda\rangle = v_{q\lambda}^{j\alpha}(\vec{R}_j) = \frac{1}{\sqrt{N}} \exp(i\vec{q}\cdot\vec{R}_j)\epsilon_{q\lambda}^{j\alpha} . \quad (2)$$

Here the $\{\vec{q}\}$ form a set of N wave vectors in the first Brillouin zone, λ is the polarization index, and $\vec{R}_j$ is the position vector of the jth atom. The $\epsilon_{q\lambda}^{j\alpha}$ are the components of the polarization vector for mode $(q\lambda)$ which is orthonormal,

$$\sum_{j\alpha} (\epsilon_{q\lambda}^{j\alpha})^T \epsilon_{q\lambda'}^{j\alpha} = \delta_{\lambda\lambda'} . \quad (3)$$

The Green's-function matrix for the unperturbed crystal is given by

$$\underline{G}_0(\omega^2) = \frac{1}{\underline{A} - \omega^2 \underline{I}} = \sum_{q\lambda} \frac{|q\lambda\rangle\langle q\lambda|}{\omega_{q\lambda}^2 - \omega^2} . \quad (4)$$

The component form of Eq. (4) can be obtained using Eq. (2) as

$$\underline{G}_0(R_j, R_{j'}) = \frac{1}{N} \sum_{q\lambda} \frac{\exp[i\vec{q}\cdot(\vec{R}_j - \vec{R}_{j'})]}{\omega_{q\lambda}^2 - \omega^2} (\epsilon_{q\lambda}^{j\alpha})^T \epsilon_{q\lambda}^{j'\alpha} . \quad (5)$$

B. Raman-scattering intensity

Harley *et al.*[7] have shown that the Raman-scattering intensity for the first-order Stokes scattering at frequency $\omega_s = \omega_i + \omega$ is given by

$$I_{\alpha\gamma,\beta\delta}(-\omega) = \frac{\hbar}{\pi} \mathrm{Im} \sum \underline{G}_{B0}(\Gamma_i, tt')(\underline{P}_{\alpha\gamma})^T \xi(\Gamma_i t)(\underline{P}_{\beta\delta})^T \xi(\Gamma_i t') . \quad (6)$$

Here $\underline{G}_0(\Gamma_i, tt') = \xi(\Gamma_i t) G_0 \xi(\Gamma_i t')$ is an element of the Green's-function matrix given by Eq. (5) but expressed in a symmetry basis for irreducible representation Γ_i of the O_h point group. The sums over t and t' run over the symmetry basis vectors $\underline{\xi}(\Gamma_i t)$ belonging to Γ_i. The component $P_{\alpha\beta}(m\gamma) \equiv [\delta P_{\alpha\beta}/\delta v(m\gamma)]$ of $\underline{P}_{\alpha\beta}$ are first derivatives of the static polarizability tensor with respect to nuclear displacements. We assume that the elements of $\underline{P}_{\alpha\beta}(m\gamma)$ are nonzero for the defect's nearest, second-nearest, third-nearest, and fourth-nearest neighbors. The scattering from E_g mode is proportional to $I_{11} - I_{12}$, where $I_{11} = I_{xx,xx}$ and $I_{12} = I_{xx,yy}$. Thus one obtains from Eq. (6)

$$I(E_g) = \frac{2\hbar}{\pi} \mathrm{Im} \sum_{ij} P_i P_j \underline{G}_{B0}(E_g, ij). \quad (7)$$

The parameters P_i's are expressed as $P_i \equiv P_{xx}^T \underline{\xi}(E_g i)$, where i runs from 1 to 6. This is because there are six E_g modes, one from the nearest, two from the second-nearest, one from the third-nearest, and two from the fourth-nearest neighbors. Some of these basis vectors are tabulated in Ref. 5.

C. Perturbed phonons

For the case of perturbed E_g phonons, one considers the longitudinal-force-constant changes δf_l between the defect and its six nearest neighbors. One can write the Raman-scattering intensity from $\mathrm{Im}G(E_g)$, which is expressed as

$$\mathrm{Im}G(E_g) = \frac{\mathrm{Im}G_{B0}(E_g)}{(1 + \delta f_l \,\mathrm{Re}G_{B0})^2 + (\delta f_l \,\mathrm{Im}G_{B0})^2} , \quad (8)$$

where

$$\mathrm{Re}G_{B0}(E_g, \omega^2) = \frac{1}{\pi} \mathrm{P} \int_0^{\omega_m^2} \frac{\mathrm{Im}G_{B0}(E_g, \omega'^2)}{\omega'^2 - \omega^2} d\omega'^2 .$$

Gethins *et al.*[6] assume changes in the force constants between the defect ion and its first-nearest neighbors (δf_l) as well as first- and fourth-nearest neighbors (δg_l). We have also examined this model as an alternative method to calculate the theoretical spectrum.

III. EXPERIMENTAL RESULTS AND DISCUSSION

A. Experimental spectra

The defect-ion (Co^{2+}) concentration in the MgO crystal is approximately 2500 ppm as quoted by its manufacturer, W. & C. Spicer Ltd. The incident and scattered lights are propagated along the [001] and [110] directions of the crystallographic axes. This particular choice of the propagation directions allows us to observe the spectrum in the E_g polarization geometry with the incident ($\vec{\epsilon}_i$) and scattered ($\vec{\epsilon}_s$) polarization vectors along the [110] and [1$\bar{1}$0] directions. The spectra have been recorded with a Spex 1400 double monochromator using the 5145-Å wavelength of the argon-ion laser source. The signal is collected by a photomultiplier, picoammeter, and is finally plotted on a X-Y chart recorder. The sample is mounted inside a cryostat of the closed cycle refrigeration system by Air Products. We have been able to control the temperature from 18 °K to room temperature with an accuracy of ± 2 °K. The E_g spectrum at 18 °K is shown in Fig. 1.

The temperature dependences of the three peaks at 278.5, 304.75, and 935.7 cm^{-1} are shown in Fig. 2. The T_{2g} spectrum in this sample is weak and is not shown.

B. Energy-level scheme of the CO^{2+} ion in cubic symmetry

The ground electronic state of the Co^{2+} ion in a cubic field is an orbital triplet ($^4T_1$). First-order spin-orbit coupling splits the ground electronic

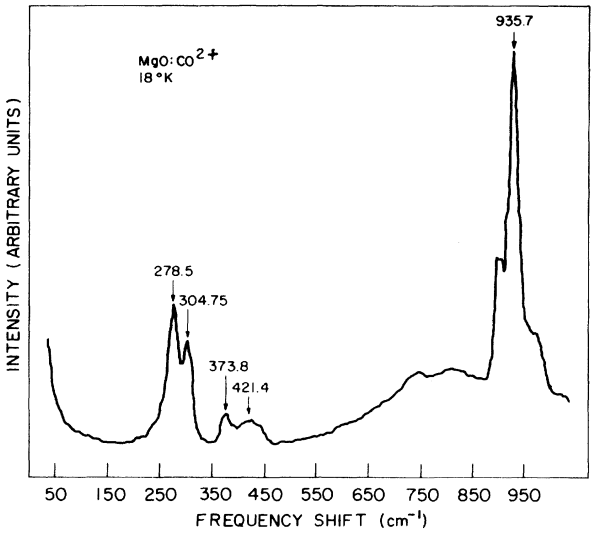

FIG. 1. E_g spectrum at 18° K. The peaks at 278.5 cm^{-1}, 304.75 cm^{-1}, 373.8 cm^{-1} and 421.4 cm^{-1} are the one-phonon spectrum. The peak at 935.7 cm^{-1}, which is superimposed on the two-phonon spectrum of pure MgO, is identified as the $\tau_6 \rightarrow \tau_8^2$ electronic transition between the low-lying energy levels of the Co^{2+} ion.

state into two Kramer doublets (τ_6, τ_7) and two quartets ($\tau_8^{1,2}$). The separation between the energy levels has been calculated by Mann *et al.*[8] and is shown in Fig. 3. From the temperature dependence of the 935.7-cm^{-1} peak, we assign it to the

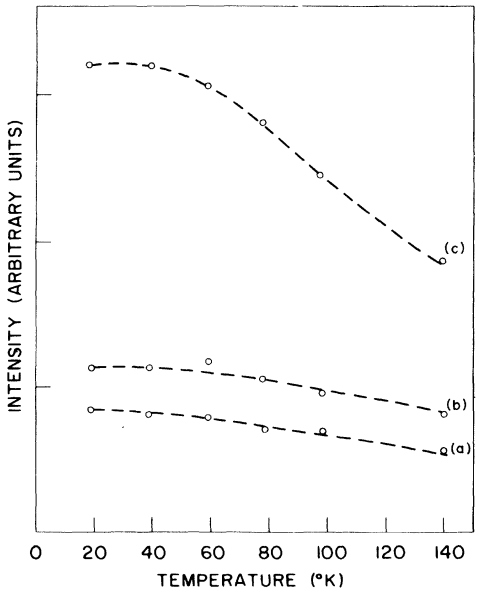

FIG. 2. Temperature dependence of the peaks at (a) 304.75 cm^{-1}, (b) 278.5 cm^{-1}, (c) 935.7 cm^{-1}. The intensity of one-phonon peaks at 278.5 cm^{-1} and 304.75 cm^{-1} obey the $1-\exp(-\hbar\omega/kT)$ law. The experimental points are joined for convenience.

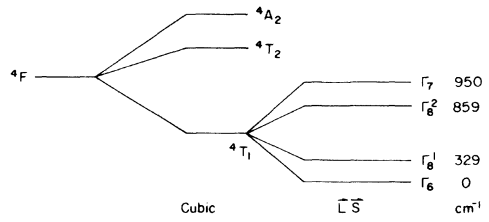

FIG. 3. Low-lying energy levels of Co^{2+} ion in cubic field with spin-orbit coupling ($\vec{L}\cdot\vec{S}$). Calculated values are quoted from Ref. 8.

$\tau_6 \rightarrow \tau_8^2$ electronic transition. According to calculations, a peak should also appear at ~300 cm^{-1} due to the $\tau_6 \rightarrow \tau_8^1$ transition. Why it did not appear in the experimental spectrum is not very clear. The temperature-dependent behavior of the peaks at 278.5 and 304.75 cm^{-1} clearly ruled out the possibility that their origins were of an electronic nature. We plan to investigate the electronic Raman scattering in this system in the presence of a magnetic field in the near future.

C. Calculations with unperturbed phonons

The frequencies and the polarization vectors of the host lattice are obtained with the BSM calculations of Sangster *et al.*[3] In this model, the unperturbed vibrational frequencies and core polarization vectors have been calculated for a uniform mesh of 1686 points in a 1/48 section of the Brillouin zone from a fit to the neutron-scattering data. We have used these eigenvectors to calculate the $\mathrm{Im}G_{B0}(E_g, ij)$ for the six E_g displacements due to the first-, second-, third-, and fourth-nearest neighbors. They are then sorted out into 100 bins of equal width with appropriate weightage factors. Independent contributions of the E_g displacements to the $\mathrm{Im}G_{B0}(E_g, ij)$ are shown in Fig. 4. The inclusion of the two E_g modes arising from the vibrations of the second-nearest neighbors which are twelve magnesium ions enhances the intensity of the acoustic peak at 304 cm^{-1} and the optic mode at 421 cm^{-1} as compared to the nearest-neighbor coupling calculations. In order to produce an agreement in the line shape between theory and experiment, we have combined the five E_g displacements in accordance with Eq. (7). The second E_g mode coming from the fourth-nearest-neighbor displacements has been ignored because the inclusion of this mode, which is out of phase with the first-nearest neighbor displacements, enhances the intensity of the optic mode and deteriorates the agreement between theory and experiment. In Fig. 5(b) we show the calculated intensity for the combined E_g displacements. It is to be noted that we have assumed the electron-phonon coupling to be the same for all five modes. In Fig.

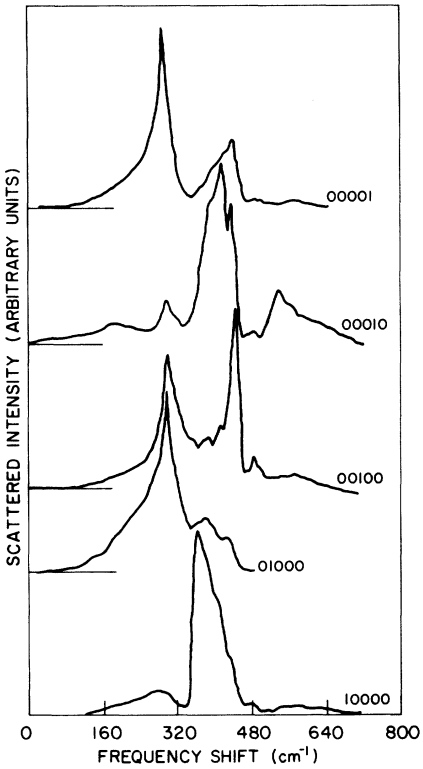

FIG. 4. Theoretical E_g spectra for first (10000)–, second (01000,00100)–, third (00010)–, and fourth (00001)–nearest neighbors of the defect with unperturbed phonons of the BSM. Here the indices correspond to the electron-phonon coupling strength P_i.

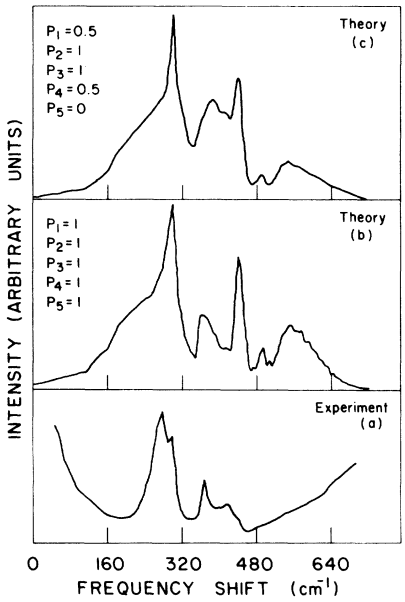

FIG. 5. Theoretical and experimental E_g spectra. The calculated spectra are: (b) the combined E_g displacements which include defect's first-, second-, third-, and fourth-nearest neighbors, with unperturbed lattice phonons, (c) the same as (b) without fourth-nearest neighbor displacements, but with different coupling parameters.

5(c) fractional values of P_1 and P_4 are taken which also lead to a good agreement between theory and experiment. For both sets of values P_i we have been able to achieve a good agreement between theory and experiment, except for the peak at 278.5 cm^{-1} which we attribute to a local mode.

D. Perturbed-phonon model

As an alternative model, we also examine the change in longitudinal force constants between the defect and its nearest neighbors. The line shapes for a change of nearest-neighbor force constants of 4% and 8% are shown in Fig. 6. A local mode appears at 278.5 cm^{-1}, but the line shapes and peak positions for other modes are in poor agreement with experiment. We have also examined the model of Gethins *et al.*,[6] in which a longitudinal-force-constant change between the nearest and fourth-nearest neighbors has been assumed. Unfortunately, this model does not lead to any significant change in the line-shape spectrum for about 20% change in the force constant between defect's first- and fourth-nearest neighbor. This is shown in Fig. 7. Any further changes in force constants worsen the line-shape profile.

IV. CONCLUSION

We have found that the inclusion of second-, third-, and fourth-nearest-neighbor displacements in electron-phonon interaction results in a good agreement between theory and experiment as compared to the nearest-neighbor coupling model. We have also examined the perturbed-phonon model of Gethins *et al.*[6] in which the change in positions of nearest and fourth-nearest neighbors of the defect gives rise to a change in force constant between them. We have found this model to be unsatisfactory. Robbins *et al.*[5] have also achieved a good agreement between theory and experiment when defect's second-nearest-neighbor displacements are included in calculations as compared to the nearest-neighbor coupling and perturbed-phonon models. The strong evidence of the superiority of the electron-phonon coupling model with defect coupled to displacements of distant neighbors, over the complicated perturbed-phonon model, suggests that it would probably be of scientific interest to calculate the strength of the electron-phonon interaction as a function of displacements of nearest as well as distant neighbors. It has been shown[4] that

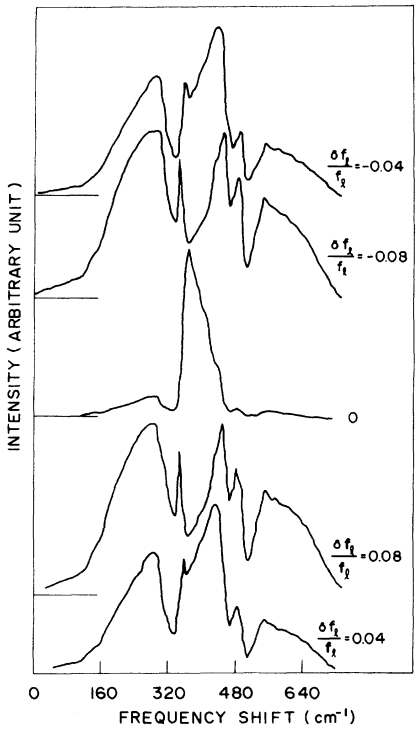

FIG. 6. Perturbed theoretical E_g spectra for nearest-neighbor force constant change model. The fractional-force-constant changes ($\delta f_1/f_1$) are indicated on the side of each curve. The value of f_1 is taken as the unperturbed nearest-neighbor overlap (shell-shell) longitudinal force constant $\frac{1}{2}A$ of the BSM.

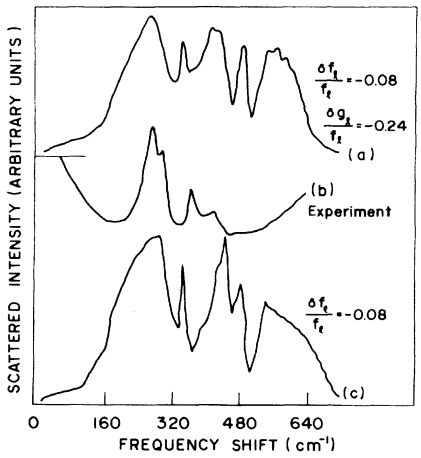

FIG. 7. (a) Perturbed theoretical E_g spectrum for changes in longitudinal force constants between defect and its nearest (δf_1) as well as nearest and fourth-nearest (δg_1) neighbors, (b) E_g Raman spectrum at 18° K, (c) perturbed theoretical E_g spectrum for changes in longitudinal force constants between defect and its nearest neighbors only.

for Jahn-Teller ions which are strongly coupled to the lattice, the displacements of distant neighbors fall off as $\sim 1/r^2$ where r is the distance of neighboring ions from the defect. Therefore the inclusion of second-, third-, and fourth-nearest-neighbor displacements in our calculations is probably justified. How strongly these distant neighbors are coupled to the defect is a conundrum. It requires a systematic study of impurity-induced vibrations of ions which are strongly coupled to the lattice (e.g., Fe^{2+}, Cu^{2+}, Mn^{3+}, etc., in CaO or MgO) along with weakly coupled ion-lattice systems. We have also observed a peak at 935.7 cm^{-1} due to electronic transition $\tau_6 \rightarrow \tau_8^2$ between energy levels of Co^{2+} ion.

ACKNOWLEDGMENTS

I wish to thank Professor S. P. S. Porto for inviting me to UNICAMP, Brazil. I also thank Professor R. S. Katiyar for providing his laboratory facilities to me. Finally, I would like to express my gratitude to José Claudio Galzerani for his assistance in the laboratory. This research was supported by FAPESP of São Paulo, Brazil, Grant No. 77-0896.

[1]A. Billat, J. P. Mon, and M. Voisin, Phys. Status Solidi B 67, 335 (1975).
[2]U. Schröder, Solid State Commun. 4, 347 (1966).
[3]M. J. L. Sangster, G. Peckham, and D. H. Saunderson, J. Phys. C 3, 1026 (1970).
[4]S. Guha and L. L. Chase, Phys. Rev. B 12, 1658 (1975).
[5]D. Robins and J. B. Page, Phys. Rev. B 13, 3604 (1976).
[6]T. Gethins, T. Timsuk, and E. J. Woll, Phys. Rev. 157, 744 (1967).
[7]R. T. Harley, J. B. Page, and C. T. Walker, Phys. Rev. B 3, 1365 (1971).
[8]A. J. Mann, P. J. Stephens, Phys. Rev. B 9, 863 (1974).